




# Utility-based operation management for low voltage distribution grids using online optimization

H. Ipach , L. Fisser , C. Becker, A. Timm-Giel 

We present an operation management controller for low voltage (LV) grids that coordinates a multitude of distributed energy resources (DER) in real time to maximize the utilization of renewable energy production. It utilizes an LTE radio network that connects the DERs to the distribution system operator. In our approach, utility functions are assigned to the DERs, and the utility maximization is formulated as an optimization problem. The optimization problem is solved by an iterative algorithm that performs incremental updates of the DER power set values to achieve the optimum. In order to take the state of the grid in the optimization process into account, the state of the grid is estimated. During the simulation of a use case, we demonstrate the applicability and identify the benefits of our approach compared to an established optimal power flow (OPF) method. Particular emphasis is put on evaluating the communication delay and feasibility of the required communication network, as the iterative approach leads to a high communication load.

**Keywords:** smart grid; distributed energy resources; optimal power flow; 450 MHz LTE

## **Nutzenbasierte Betriebsführung von Niederspannungs-Verteilnetzen mittels Online-Optimierung.**

*Wir stellen einen Betriebsführungsregler für Niederspannungsnetze vor, der eine Vielzahl dezentraler Energieanlagen (DEA) in Echtzeit koordiniert, um die Nutzung der erneuerbaren Energieerzeugung zu maximieren. Der Regler verwendet ein LTE-Funknetzwerk, das die DEA mit dem Verteilnetzbetreiber verbindet. In unserem Ansatz werden den DEA Nutzenfunktionen zugewiesen und die Nutzenmaximierung wird als Optimierungsproblem formuliert. Das Optimierungsproblem wird durch einen iterativen Algorithmus gelöst, der inkrementelle Anpassungen der Leistungssollwerte der DEA in Richtung des Optimums vornimmt. Um den Netzzustand im Optimierungsprozess zu berücksichtigen, wird dabei eine Netzzustandsschätzung verwendet. In der Simulation eines Anwendungsfalls demonstrieren wir die Anwendbarkeit und identifizieren Vorteile unseres Ansatzes im Vergleich zu einem etablierten Optimal-Power-Flow-Verfahren. Ein besonderes Augenmerk liegt dabei auf der Evaluation der Kommunikationslaufzeit sowie der Umsetzbarkeit des benötigten Kommunikationsnetzes, da der iterative Ansatz eine hohe Kommunikationslast bedingt.*

**Schlüsselwörter:** Smart Grid; dezentrale Energieanlagen; Optimal Power Flow; 450 MHz LTE

Received July 19, 2021, accepted September 6, 2021, published online September 17, 2021  
© The Author(s) 2021



## 1. Introduction

On the way towards a zero-emission energy supply, a multitude of new distributed energy resources (DER) and controllable loads are being connected to existing low voltage (LV) distribution grids. For ease of presentation, we refer to both DERs and controllable loads as DERs. With DERs, formerly passive consumers become active *prosumers* who may inject or consume electric power depending on the circumstances. Common types of DERs are e.g. photovoltaic (PV) power plants, battery electric vehicles (BEV) and heat pumps (HP). While PV plants are supposed to supply an important part of the electric energy demand in the future grid, BEVs and HPs are new kinds of consumers that result from the increasing electrification of the mobility and heat sectors. From the viewpoint of LV grid operation, a largely uncontrolled installation and operation of DERs is undesired due to the risk of congestion in peak load or peak infeed situations. In this context, congestions include voltage limit violations as well as excess currents exceeding the thermal limits [1, 2]. Therefore, new concepts are required of how to control the DERs in such a way that congestions are avoided on one hand and the volatile regenerative energies are utilized in an optimal fashion on the other hand.

Currently, control schemes for the coordinated operation of DERs in German LV grids are not widely implemented. One obstacle is the lack of the communication network and metering infrastructure that coordinated control schemes require. In this regard, a cornerstone towards higher grid state transparency and higher controllability is the smart meter rollout. In addition, the adaptation of the regulatory framework to exploit the flexibility of DERs in order to avoid grid congestion is actively discussed in research and politics. To date, the regulatory framework in Germany already permits distribution system operators to charge reduced network fees to customers with DERs that agree to a grid-oriented control of their assets [3].

Within this paper, we present a LV grid operation management method that coordinates the operation of DERs in respect of the

---

**Ipach, Hanko**, Institute of Electrical Power and Energy Technology (iinet), Hamburg University of Technology, Harburger Schloßstraße 36, C2/C3, 21079 Hamburg, Germany (E-mail: [Hanko.Ipach@tuhh.de](mailto:Hanko.Ipach@tuhh.de)); **Fisser, Leonard**, Institute of Communication Networks (ComNets), Hamburg University of Technology, Hamburg, Germany; **Becker, Christian**, Institute of Electrical Power and Energy Technology (iinet), Hamburg University of Technology, Hamburg, Germany; **Timm-Giel, Andreas**, Institute of Communication Networks (ComNets), Hamburg University of Technology, Hamburg, Germany

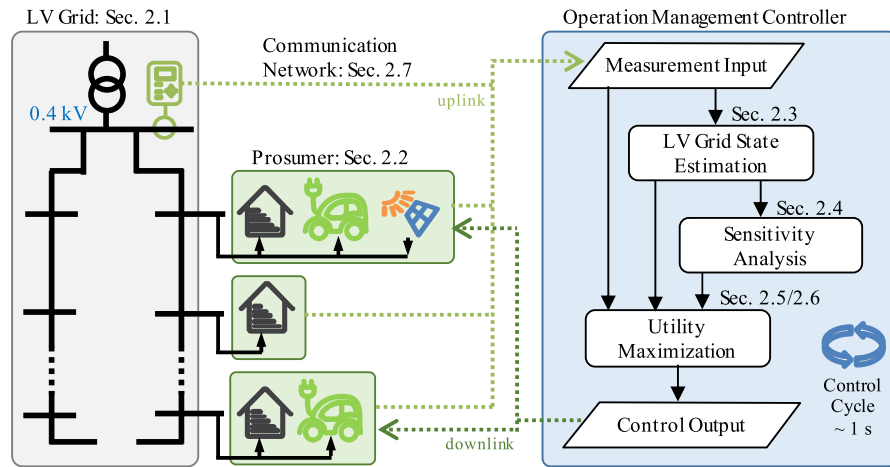


Fig. 1. Schematic diagram of the data exchanged and algorithms employed in the operation management controller

limited grid capacity. Thus, it is designed for the power system of tomorrow, when the amount of installed DERs necessitate their coordinated control on the one hand, and a metering and communication infrastructure is established on the other hand. In the following chapter, the methodology is explained in detail.

## 2. Operation management controller

The proposed operation management scheme can be categorized as an optimal power flow (OPF) method. It derives the active and reactive power set values for the DERs from an optimization problem that is constrained by limits imposed by the DERs and the LV grid. In contrast to the classical OPF formulation, consumers and generators are considered in one common framework. Furthermore, instead of minimizing the generation costs, we quantify a *utility* of both consumed and generated active power and maximize its overall value. The utility expresses the benefit that a DER experiences from a certain power consumption or injection. While algorithmically the interpretation of the optimization variables is merely a definition issue, the utility formulation allows to generalize from actual costs. The resulting optimization problem is then solved by an online optimization that iteratively adjusts the power set values towards their optimal values. In each iteration, it utilizes the most recent measurement feedback from the grid. In this way it differs from classical offline optimization algorithms that only forward output values upon convergence. Due to advantages like a low complexity and a high robustness against modelling errors, online optimization has gained a lot of interest recently, especially in the context of OPF [4–6]. The algorithm utilized here is based on the framework proposed in [4]. We adapt the saddle point flow method proposed therein and complement it by a state estimation. As a result, our method allows to consider constraints on grid state variables that are not directly measured. The combination of online optimization and SE for OPF has been investigated in [7], where a Kalman-filter based SE is utilized. In contrast to [7], we employ the modified branch-current based SE proposed in [8] that avoids repeated matrix inversions and thus keeps the computational complexity low. Furthermore, an emphasis is placed on the accurate communication system modelling. The fast and reliable communication of measurement and control values is of special interest in online optimization applications, as the iterative procedure necessitates a short control cycle to achieve fast convergence.

Figure 1 provides an overview of the data flows and the algorithms employed in the proposed operation management. The following sections describe the individual parts in detail (note the references in Fig. 1). At first, the grid model and relevant operational constraints are explained in Sect. 2.1. Section 2.2 then elaborates on the prosumer and DER models. Afterwards, Sects. 2.3 to 2.6 refer to the individual functions within the operation management controller, which are executed with a cycle time of one second. The first two of these sections contain brief descriptions of the SE and the subsequent sensitivity analysis, both of which are functions required to consider grid constraints in the optimization. The utility formulation and the resulting optimization problem are addressed in Sects. 2.5 and 2.6, respectively. Finally, the derivation of communication network characteristics is explained in Sect. 2.7.

### 2.1 Grid topology and operational constraints

Most commonly, German low voltage grids are of the four-wire three-phase type. With regards to the topology, they are typically operated as radial grids with a single transformer connection to the superordinate medium voltage (MV) grid. Less frequently, meshed structures and/or multiple transformer connections can be encountered – usually in areas with high load density [9]. Here, we focus on the first type. The LV grid's topology is thus modelled as a tree graph  $\mathcal{G} = (\mathcal{N}, \mathcal{E})$  with the set of nodes  $\mathcal{N} = \{0, 1, \dots, N+1\}$ , where 0 denotes the slack node, and the set of distribution lines  $\mathcal{E} = \{(n_1, n_2) \mid n_1, n_2 \in \mathcal{N}\}$ . Furthermore, let  $\mathcal{N}_+ = \mathcal{N} \setminus \{0\}$  denote the set of nodes excluding the medium voltage side of the transformer, which is assumed to be the slack node.

The operational boundaries considered here are related to steady-state node voltages and line currents. Let  $v_i^\phi(t)$  denote the time-varying complex voltage phasor of phase  $\phi$  at node  $i \in \mathcal{N}_+$ , and  $i_k^\phi(t)$  the complex current phasor of phase  $\phi$  of line  $k \in \mathcal{E}$ . While the node voltage magnitude at customer connection points should remain within a specified interval  $[\underline{v}, \bar{v}]$  under normal operating conditions, line currents (and the transformer current) are restricted to values below the thermal limits  $i_{k,N}$ ,  $k \in \mathcal{E}$  to prevent equipment overheating. Thus,

$$\underline{v} \leq |v_i^\phi(t)| \leq \bar{v} \quad \forall i \in \mathcal{N}_+, \phi \in \{L1, L2, L3\} \quad \text{and} \quad (1)$$

$$|i_k^\phi(t)| \leq i_{k,N} \quad \forall k \in \mathcal{E}, \phi \in \{L1, L2, L3\} \quad (2)$$

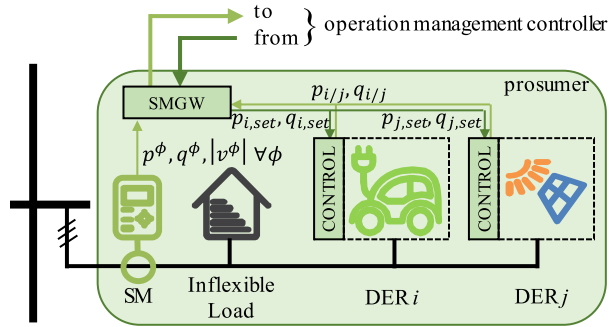


Fig. 2. Measurement and control value processing within an exemplary prosumer containing two DERs. SM = smart meter, SMGW = smart meter gateway

are constraints imposed by the power grid. It should be noted that further issues may arise from the large-scale integration of inverter-based DERs with regards to power quality. For example, the Total Harmonic Distortion (THD) might increase above admissible limits [10]. Such power quality issues that relate to harmonic frequencies are not addressed here. Furthermore, voltage imbalance can be an issue in LV grids due to an uneven assignment of single phase consumers or generators [11]. Although our controller does not actively balance the voltage, the three-phase monitoring included in the operation management allows to detect voltage imbalances.

## 2.2 Prosumer and DER modelling

With regards to DERs, we make some definitions for clarity. We define a prosumer as the owner of one or more DERs. A prosumer contains at most one inflexible load as well as any number of DERs. The inflexible load e.g. summarizes common residential load that cannot be controlled by the operation management. Each DER, on the contrary, provides the possibility to adjust its active and reactive power set values within ranges that may vary over time. Thus, denoting the set of all DERs connected to the LV grid by  $\mathcal{C}$ ,

$$p_c(t) \in [\underline{p}_c(t), \bar{p}_c(t)] \quad \text{and} \quad (3)$$

$$q_c(t) \in [\underline{q}_c(t), \bar{q}_c(t)] \quad \forall t, \forall c \in \mathcal{C}. \quad (4)$$

With regards to the sign of  $p$  and  $q$ , we define that positive power values denote injections into the grid. For an electric vehicle charger with a diode inverter front end, for instance, the upper limit of the active power range is zero and the lower limit depends on the battery's state of charge (SOC). In general, three-phase connected DERs are assumed to be wye-connected and to inject symmetric current. Note that (3) and (4) imply that both active and reactive power can take any value within the range. Therefore, DERs with discrete power levels are excluded.

Every DER of the LV grid that participates in the operation management communicates its actual active and reactive power values to the controller. In return, it receives active and reactive power set values. In addition, we assume that each prosumer contains a smart metering device that transmits power and voltage measurements of each phase via a smart meter gateway (SMGW). Depending on the location of the smart meter (SM), the power measurements either summarize the prosumer's inflexible and flexible load, as shown in Fig. 2, or contain only the inflexible load. In any case, we assume that the total prosumer power can be determined from the SM and DER measurements.

## 2.3 State estimation

Besides the measurement values from prosumers, our controller can process further measurements e.g. from the substation or cable distribution cabinets, if available. Upon arrival at the controller, all available measurements are forwarded to a state estimation (SE) algorithm. The SE task is to compute a consistent grid state from all available measurements that fulfils the power flow equations on one hand and minimizes a certain distance to the measurements on the other hand [12]. In the conventional SE applied in transmission grids, the grid state is expressed in terms of the node voltage phasors. Stacking up the nodal power injections of all phases in the vectors  $\mathbf{p} \in \mathbb{R}^{3 \cdot N}$  and  $\mathbf{q} \in \mathbb{R}^{3 \cdot N}$  and the line-to-neutral node voltage phasors in the vector  $\mathbf{v} \in \mathbb{C}^{3 \cdot N}$ , the three-phase AC power flow equations at a discrete time  $t_k, k \in \mathbb{N}$  can be written as

$$\mathbf{p}(t_k) + j\mathbf{q}(t_k) = \text{diag}(\mathbf{v}(t_k)) \cdot \text{conj}(\mathbf{Y}_{01}^T \mathbf{v}_0(t_k) + \mathbf{Y}_{11} \mathbf{v}(t_k)), \quad (5)$$

where  $j$  is the imaginary unit,  $\mathbf{v}_0 \in \mathbb{C}^3$  denotes the slack node voltage,  $\mathbf{Y}_{01} \in \mathbb{C}^{3 \times 3N}$  and  $\mathbf{Y}_{11} \in \mathbb{C}^{3N \times 3N}$  are submatrices of the nodal admittance matrix

$$\mathbf{Y} = \begin{bmatrix} \mathbf{Y}_{00} & \mathbf{Y}_{01} \\ \mathbf{Y}_{01}^T & \mathbf{Y}_{11} \end{bmatrix} \in \mathbb{C}^{(3N+3) \times (3N+3)}, \quad (6)$$

$\text{diag}(\cdot)$  converts a vector to a diagonal matrix and  $\text{conj}(\cdot)$  takes the complex conjugate.

While  $\mathbf{v}_0$  and  $\mathbf{v}$  fully define the stationary grid state, this choice of state variables is not unique. Here, we utilize a branch-current based approach instead, which expresses the grid state in terms of the line current phasors  $\mathbf{i} \in \mathbb{C}^{3 \cdot |\mathcal{E}|}$ . Employing Ohm's law, the node voltage phasors are then derived from the line currents. Especially for radial distribution grids, branch-current based approaches have gained popularity, mainly due to their computational efficiency [13]. More specifically, we apply the modified branch-current based SE proposed in [8]. It consecutively solves linear weighted-least-squares (WLS) problems until the estimated line current phasors converge. Due to the linear formulation, the computational complexity is significantly reduced compared to standard WLS approaches. This allows for short computation times even in unbalanced three-phase grids.

Without any further measurements, the SE method at least requires the active and reactive power of all prosumers to achieve observability. In case of unobserved prosumers, i.e. the ones without a smart meter, actual measurements are not available. For these unobserved prosumers, we assume that at least their annual energy consumption is known. Then, scaled standard load profiles (SLP) are used as pseudo-measurements with low weighting factors, which is a common approach to gain observability in distribution grid SE with sparse measurements [7]. The power factor is assumed to equal 0.95. Even when further measurements are available, the pseudo-measurements are kept to reach measurement redundancy.

## 2.4 Sensitivity analysis

The outputs of the state estimation algorithm are the estimated line current phasors  $\mathbf{i} \in \mathbb{C}^{3 \cdot |\mathcal{E}|}$  as well as the phase-to-neutral node voltage phasors  $\mathbf{v}_0 \in \mathbb{C}^3$  and  $\mathbf{v} \in \mathbb{C}^{3 \cdot N}$ . In the controller, on one hand they are used to determine the maximum and minimum phase-to-neutral voltages and currents at all nodes. These are directly forwarded to the utility maximization, where they are required to assess if any limit violations are present. On the other hand, the voltage phasors are input to a *sensitivity analysis* function. The purpose of this function is to compute approximate linear mappings of nodal

active and reactive power changes to node voltage and line current magnitudes. As we consider balanced three-phase DERs, we restrict the sensitivity analysis to the positive sequence node voltage and line current phasors and denote them by  $\mathbf{v}^{ps}(t_k) \in \mathbb{C}^N$  and  $\mathbf{i}^{ps}(t_k) \in \mathbb{C}^{|\mathcal{E}|}$ , respectively (note that the slack node is excluded in  $\mathbf{v}^{ps}$ ). Hence, matrices  $S_{PV}(t_k), S_{QV}(t_k) \in \mathbb{R}^{N \times N}$  and  $S_{PI}(t_k), S_{QI}(t_k) \in \mathbb{R}^{|\mathcal{E}| \times N}$  are computed such that

$$\begin{bmatrix} \Delta |\mathbf{v}^{ps}| \\ \Delta |\mathbf{i}^{ps}| \end{bmatrix} \approx \begin{bmatrix} S_{PV}(t_k) & S_{QV}(t_k) \\ S_{PI}(t_k) & S_{QI}(t_k) \end{bmatrix} \cdot \begin{bmatrix} \Delta \mathbf{p} \\ \Delta \mathbf{q} \end{bmatrix}. \quad (7)$$

where  $\Delta \mathbf{p}, \Delta \mathbf{q} \in \mathbb{R}^N$  denote incremental changes of the nodal injected and reactive power. As will be detailed later, these linear mappings are required by the online optimization algorithm to assess the effect of power changes on voltage and current magnitudes.

Several methods are proposed in literature to derive such linear mappings from the nonlinear power flow equations. The most straightforward one is to compute the first-order Taylor polynomial at the operating point defined by the actual grid state [14]. While it provides the best possible local linear approximation, its computation requires to invert the power flow equation's Jacobian matrix and is thus computationally costly. Therefore, we utilize the approximation

$$\begin{aligned} \mathbf{v}^{ps}(\mathbf{p} + \Delta \mathbf{p}, \mathbf{q} + \Delta \mathbf{q}) \\ \approx \mathbf{v}^{ps}(\mathbf{p}, \mathbf{q}) + (Y_{11}^{ps})^{-1} \cdot \text{diag}(\text{conj}(\mathbf{v}^{ps}(\mathbf{p}, \mathbf{q})))^{-1} \cdot (\Delta \mathbf{p} - j \Delta \mathbf{q}), \end{aligned} \quad (8)$$

to derive the sensitivity matrices, where  $Y_{11}^{ps} \in \mathbb{C}^{N \times N}$  denotes the lower right submatrix of the positive sequence nodal admittance matrix [15, 16]. The reduced accuracy of this approach is outweighed by a significantly reduced complexity: in opposite to the Taylor method, it only requires the inversion of the constant nodal admittance matrix, which can be done in advance. The resulting sensitivity matrices are passed on to the utility optimization.

## 2.5 Utility model and optimization problem

From the measurement acquisition and state estimation, the controller is aware of the actual power values  $p_c(t_k), q_c(t_k) \forall c \in \mathcal{C}$  of all DERs as well as the grid state in terms of the estimated node voltage and line current phasors  $\mathbf{v} \in \mathbb{C}^{3 \cdot N}$  and  $\mathbf{i} \in \mathbb{C}^{3 \cdot |\mathcal{E}|}$ , respectively. Subsequently, it derives new DER active and reactive power set values in view of the operational boundaries. These new set values are derived from an optimization problem formulation: We formulate each DER's utility as a function of its active power, and strive for the maximization of the sum of all DER's utilities.

In our utility model, each DER's basic utility  $\Phi_{\text{base}}$  is a quadratic function of its active power, i.e.

$$\Phi_{\text{base},c}(p_c(t_k)) = r_c \cdot p_{N,c} \cdot \left( 1 - \left( \frac{p_c(t_k) - p_{N,c}}{p_{N,c}} \right)^2 \right), \quad c \in \mathcal{C}, \quad (9a)$$

where  $\mathcal{C}$  denotes the set of DERs,  $p_{N,c}$  the (signed) nominal power of DER  $c$ , and  $r_c$  equals  $-1$  and  $+1$  for consumers (or storages) and power plants, respectively. Note that the basic utility function takes its maximum at the DER's rated power, and it is also scaled according to the rated power. Furthermore, the utility equals zero at zero active power. Now, by means of an individual *priority* value  $w_c$  that can be set within a globally predefined range, a DER  $c$  can express its urgency of consuming or injecting active power. It should

be noted that in a real-world implementation, high priority values should be penalized e.g. by priority-dependent network charges to incentivize low priorities. The final utility of a DER is obtained by multiplying the basic utility function by its priority, i.e.

$$\Phi_c(w_c(t_k), p_c(t_k)) = w_c(t_k) \cdot \Phi_{\text{base},c}(p_c(t_k)). \quad (9b)$$

The use of this utility model, which is similar to the one proposed in [17], is motivated by several targets. On one hand, a fair allocation of the limited grid capacity is desired. This should be covered by assigning equally shaped basic utility functions to all participating DERs under consideration of the individual nominal DER powers. On the other hand, individual preferences should be taken into account. This is supposed to be achieved by the priority factors. Without having to disclose sensitive information, they allow the DERs to take e.g. expected operation schedules into account.

The utility model only considers active power and assumes the DERs themselves have no benefit from injecting or consuming reactive power. To make use of their reactive power capability for voltage control, a negative utility function

$$\Phi_Q(q_c(t_k)) = -w_Q \cdot (q_c(t_k))^2 \quad (10)$$

is assigned to reactive power with a small weighting factor  $w_Q$ . This should ensure that reactive power is preferably used to correct voltage limit violations.

Denoting the set values for all DERs by  $\mathbf{p}^c \in \mathbb{R}^{|\mathcal{C}|}$  and  $\mathbf{q}^c \in \mathbb{R}^{|\mathcal{C}|}$  and formulating the utility maximization as a minimization, the overall optimization problem at time  $t_k$  reads

$$\begin{aligned} \min_{\mathbf{p}^c(t_k), \mathbf{q}^c(t_k)} & -\Phi_{\text{tot}}(\mathbf{w}(t_k), \mathbf{p}^c(t_k), \mathbf{q}^c(t_k)) \\ = & \min_{p_c(t_k), q_c(t_k) \forall c \in \mathcal{C}} \sum_{k \in \Pi} (-\Phi_c(w_c(t_k), p_c(t_k)) - \Phi_Q(q_c(t_k))) \end{aligned} \quad (11)$$

s.t. (1)–(5).

In spite of the convex objective function, the nonconvex AC power flow equations (5) that relate voltage and current magnitudes to DER power values make (11) a nonconvex optimization problem. Off-the-shelf optimization tools are available to solve it in a classical fashion, e.g. Matpower [18]. They solve (11) based on the actual values available at a certain time  $t_k$  and a power flow model (5). Upon convergence, the optimal values are sent to the DERs. Hence, such approaches can be characterized as feedforward: they predict the voltages and currents resulting from applying the new set values solely based on the power flow model and previous input values. As shown in [6], this might result in persisting limit violations in case of an inaccurate model of the power grid. Another difficulty stems from the fact that the DER's allowed active and reactive power ranges (3)–(4) have to be known, which might not be the case especially for weather-dependent DERs like PV plants. Furthermore, the computational complexity of repeatedly solving an OPF with a high number of DERs in feedforward fashion until convergence is high. These issues are addressed in the following section.

## 2.6 Online feedback-based optimization algorithm

To avoid the drawbacks of a feedforward optimization, we utilize an online feedback-based algorithm to solve (11). Within one control cycle, it computes an incremental update towards the optimum instead of solving (11) until convergence. In the next cycle, updated

measurement values are taken into account to compute the next incremental step, which closes the control loop and justifies the term *feedback optimization*. The closed-loop approach increases the robustness to model errors. Also, the iterative procedure significantly reduces the computational burden within each control cycle compared to feedforward optimization [4–6].

Our algorithm is based on the projected gradient method proposed in [4]. It aims to solve the dual problem associated with the optimization problem (11), where DER power level constraints (3)–(4) are enforced by projection. Thus, Lagrange multipliers  $\lambda_-, \lambda_+ \in \mathbb{R}^N$  and  $\mu \in \mathbb{R}^{|\mathcal{E}|}$  are introduced for the lower and upper voltage and current constraints (1) and (2), respectively, to formulate the (partial) Lagrangian

$$\begin{aligned} \mathcal{L}(\mathbf{p}^c, \mathbf{q}^c, \lambda_-, \lambda_+, \mu) \\ = -\Phi_{\text{tot}}(\mathbf{w}, \mathbf{p}^c, \mathbf{q}^c) + \lambda_-^\top (\underline{\mathbf{v}} - |\mathbf{v}^{\text{ps}}|) + \lambda_+^\top (|\mathbf{v}^{\text{ps}}| - \bar{\mathbf{v}}) \\ + \mu^\top (|\mathbf{i}^{\text{ps}}| - \mathbf{i}_N), \end{aligned} \quad (12)$$

where  $\underline{\mathbf{v}}, \bar{\mathbf{v}} \in \mathbb{R}^N$  and  $\mathbf{i}_N \in \mathbb{R}^{|\mathcal{E}|}$  denote vectors containing the node voltage and branch current limits (cf. (1)–(2)), and the time dependencies have been dropped for simplicity. The dual problem then reads

$$\max_{\lambda_-, \lambda_+, \mu} \left( \min_{\mathbf{p}^c, \mathbf{q}^c} \mathcal{L}(\mathbf{p}^c, \mathbf{q}^c, \lambda_-, \lambda_+, \mu) \right), \quad (13)$$

which constitutes a saddle-point problem. To iteratively approach the saddle-point over time by taking incremental steps towards the optimum, a primal-dual projected gradient method is employed. The update rules read

$$\lambda_+(t_{k+1}) = \Pi_{\mathbb{R}_+^N} [\lambda_+(t_k) + \alpha_v \cdot (|\mathbf{v}^{\text{ps}}(t_k)| - \bar{\mathbf{v}})], \quad (14a)$$

$$\lambda_-(t_{k+1}) = \Pi_{\mathbb{R}_+^N} [\lambda_-(t_k) + \alpha_v \cdot (\underline{\mathbf{v}} - |\mathbf{v}^{\text{ps}}(t_k)|)], \quad (14b)$$

$$\mu(t_{k+1}) = \Pi_{\mathbb{R}_+^{|\mathcal{E}|}} [\mu(t_k) + \alpha_i \cdot (|\mathbf{i}^{\text{ps}}(t_k)| - \mathbf{i}_N)], \quad (14c)$$

$$\begin{aligned} \mathbf{p}_{unc}^c(t_{k+1}) &= \mathbf{p}^c(t_k) + \alpha \cdot (\nabla_{\mathbf{p}^c} \Phi_{\text{tot}}(t_k) - S_{PV}^\top(t_k) \\ &\quad \times (\lambda_+(t_{k+1}) - \lambda_-(t_{k+1})) - S_{PI}^\top(t_k) \cdot \mu(t_{k+1})), \end{aligned} \quad (14d)$$

$$\begin{aligned} \mathbf{q}_{unc}^c(t_{k+1}) &= \mathbf{q}^c(t_k) + \alpha \cdot (\nabla_{\mathbf{q}^c} \Phi_{\text{tot}}(t_k) - S_{QV}^\top(t_k) \\ &\quad \times (\lambda_+(t_{k+1}) - \lambda_-(t_{k+1})) - S_{QI}^\top(t_k) \cdot \mu(t_{k+1})), \end{aligned} \quad (14e)$$

$$\mathbf{p}^c(t_{k+1}) = \Pi_{[\underline{\mathbf{p}}^c(t_k), \bar{\mathbf{p}}^c(t_k)]} [\mathbf{p}_{unc}^c(t_{k+1})], \quad (14f)$$

$$\mathbf{q}^c(t_{k+1}) = \Pi_{[\underline{\mathbf{q}}^c(t_k), \bar{\mathbf{q}}^c(t_k)]} [\mathbf{q}_{unc}^c(t_{k+1})]. \quad (14g)$$

In (14a)–(14g),  $\Pi_{\mathcal{M}}[\cdot]$  denotes the projection onto the (arbitrary) set  $\mathcal{M}$ , and  $\nabla_{\mathbf{p}^c}$  the gradient with respect to  $\mathbf{p}^c$ . Furthermore,  $\alpha_v, \alpha_i, \alpha \in \mathbb{R}^{>0}$  are stepsize parameters, and  $S_\xi^\top \in \mathbb{R}^{|\mathcal{C}| \times N}$ ,  $\xi \in \{PV, PI, QV, QI\}$  denotes the transpose of the sensitivity matrix  $S_\xi$ .

It should be noted that due to the non-convex power flow equations (5), convergence of the primal-dual algorithm (14a)–(14g) towards a saddle point cannot generally be guaranteed. Therefore, a regularization term is added to the Lagrangian (12) in [4] in order to obtain analytical stability certificates. This is omitted here, as numerical results in simulations show a robust convergence in realistic power grid scenarios even without the regularization. In addition,

we utilize time-varying sensitivity matrices in (14d) and (14e) that are updated in each control cycle according to the grid state. Furthermore, the state estimation allows to consider voltage and current limits in (14a)–(14c) at all grid nodes and branches, respectively, including the ones without any actual measurement devices.

The unconstrained active and reactive power values  $\mathbf{p}_{unc}^c(t_{k+1}) \in \mathbb{R}^{|\mathcal{C}|}$  and  $\mathbf{q}_{unc}^c(t_{k+1}) \in \mathbb{R}^{|\mathcal{C}|}$  computed in (14d) and (14e) are communicated to the DER's, which concludes the control cycle. The projections onto the set of admissible powers in (14f) and (14g) are done within the DERs; as stated above, the DER power limits don't need to be known to the controller.

## 2.7 Communication network model

The operation management method relies heavily on the timely and reliable dissemination of measurement data from local SMs and power set values from the controller. It is therefore key that the underlying communication network is able to fulfil the requirements on delay bounds and update interval. However, suitable communication networks dedicated for LV grid management systems are not readily available and deployment of cellular communication infrastructure is still a technical and political challenge [19]. A promising and cost-effective approach to establish widespread coverage of dedicated cellular networks is based on LTE technology [19]. Envisioned to operate in the lower Ultra-High-Frequency (UHF) range (450 MHz) with exclusive access to 9.5 MHz of bandwidth, the 4G/5G network promises good connectivity and favourable radio properties to support large and therefore cost-effective cells [19].

The proposed operation management approach requires periodic communication in the range of one second update intervals and therefore generally favours smaller cells with higher performance. The relation between cell size (in terms of connected devices) and in-time delivery of measurements and set-points is therefore briefly investigated in the following and later integrated into the time-series simulations discussed in Chap. 3.

We define the packet loss rate (PLR) in uplink and downlink as the share of packets either exceeding the delay bound or being dropped by the network. The network topology is synthesized using a modified version of the approach presented in [20] and is described in more detail in [21]. A Geographic-Information-System such as OpenStreetMap is used to extract topology information on existing infrastructure in a region under analysis. The generation of suitable LV grid topologies is based on assumptions on typical quantities of LV consumers in LV grids presented in [22] and the fact that most of European LV lines are installed underground alongside the already existing street infrastructure.

Simulations are conducted using the LTE module of the NS-3 network simulator, configured to simulate the behaviour of a future 450 MHz LTE cellular network with six resource blocks in downlink as well as uplink. A three-sector base station is installed in the middle of the network topology. Nodes are distributed according to the topology extracted from OpenStreetMap. For each installed LV grid, one operation management controller is installed at the base station. Data packets include protocol specific information in a suitable header design, as well as the previously mentioned parameters in 32-bit resolution. The resulting packets sizes vary between 116 Byte to 128 Byte in downlink and 76 Byte to 84 Byte in uplink direction. Measurement data collected from substations is encapsulated in 216 Byte packets. Packets are sent according to the specified update interval of one second.

For evaluating the communication network's fitness to support the operation management method, the share of packets which were either lost or exceeded the one second period are considered. Both effects are summarized in node-specific PLRs.



Different network sizes were tested covering between 100 and up to 1050 actively managed SMs. These network sizes together with the assumed SM penetration of roughly 30% are in line with the assumptions on cell sizes for cost-effective deployment [19]. Increasing the number of nodes within the cell in steps of 50 showed a slow increase in PLR in uplink as well as downlink. For the smallest simulated network size of 100 nodes, no packets of any of the 36 active nodes were lost or arrived too late. For the largest network of 1050 nodes, the PLR increased to 4% in downlink and 6% in uplink on average.

Considering the small system bandwidth of just six resource blocks (out of the 25 resource blocks available in the 450 MHz band) and an update interval of one second, the performance in even the largest cell with 1050 nodes is within reasonable ranges. Especially so, if one considers the online nature of the proposed operation management system which is able to mitigate single packet losses by design. It has to be noted, that no network optimization or in depth radio channel modelling has been deployed. As such the results can only give an estimate on real world network behaviour and are generally upper bounds. Nevertheless, the results are deemed sufficiently accurate to demonstrate the operation managements feasibility.

Node-specific delays and packet losses are integrated into the time-series simulations using empirical distributions from this simulation study.

### 3. Use case

To investigate the applicability of the proposed operation management controller, we evaluate its behaviour in time-series simulations of an exemplary use case. In order to assess the combination of SE, sensitivity calculation and online optimization, the results of our controller are compared to benchmark values: assuming that all nodal powers, the slack node voltage and the DER power limits are perfectly known and communicated without delay, reference DER set values are computed using Matpower (Version 7.1) with the MIPS solver [18].

#### 3.1 Grid and prosumer specification

We use the topology of a rural-type benchmark grid from the Sim-Bench dataset [23] to test the operation management controller. While the topology as well as the distribution line and transformer specifications are taken from dataset, we modify the load and generation data to simulate a scenario for 2030. Firstly, we assume that the grid serves 74 residential consumers. To model their load, we utilize the 74 residential load profiles from [24], which feature a one-second resolution and provide individual profiles for each of the three phases. The profiles are assigned to 74 nodes within the grid. This results in an average annual energy consumption of 4685 kWh per residential consumer. Considering an average annual electric energy consumption of ~1300 kWh per person, it implies that the grid supplies ~200 people. Now, EV's and PV plants are added to certain residential consumers according to the following considerations: Today, the private vehicle density in Germany is ~570 cars per 1000 residents. Thus, assuming that the numbers of cars and residents remain constant and by 2030 every fourth car is an EV, a total number of ~30 EVs is expected in the test grid. Presuming an above-average EV throughput, we place EV chargers at 37 of the 74 residential consumers. Eighteen EVs have an 80 kWh battery and a rated charger power of 22 kW, while the others feature an 11 kW charger and a 40 kWh battery. In addition, we assume that 18 of the 37 car owners have a rooftop PV plant with rated peak powers between 15 and 20 kW. While generally the prosumers with DERs have a smart meter,

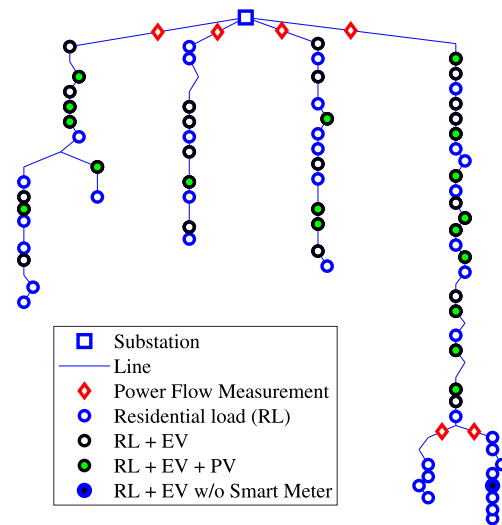


Fig. 3. Test grid topology with prosumers and power flow measurement devices

one EV charger is assumed to be installed without a metering device to simulate unmonitored “black-charging”. A schematic diagram of the resulting grid is depicted in Fig. 3. To demonstrate the effectiveness of our controller, we apply tight voltage limits of  $\underline{v} = 224$  V and  $\bar{v} = 234.4$  V, which correspond to maximum deviations of +1.5% and -3% from the rated voltage.

#### 3.2 DER capability and data exchange

As detailed in Sect. 2.2, the DER capability is described in terms active and reactive power limits. We assume that EV chargers operate at unity power factor and only allow to adjust their active power. The admissible range depends on the state of charge (SOC). As long as the SOC is between 10% and 80%, both charging and discharging at rated power is possible. The PV plants can provide both inductive and capacitive reactive power up to the amount that equals a power factor of 0.9 at rated active power. This reactive power range is available regardless of the actual active power output. The active power output of PV plants is limited by the solar irradiation, which is modelled as an upper power limit for each timestep. For the application of both active and reactive power set values, the DER controller, filter and inverter dynamics are modelled as PT1 elements with a time constant of one second.

The prosumers with SM transmit the actual DER power as well as the total prosumer power to the controller each second and participate in the operation management. On the contrary, the other 38 residential consumers are passive. We assume that these consumers do not provide any real time data, as their annual energy consumption is below 6000 kWh and therefore they are not obliged to install smart metering devices according to today's legislation [25]. Instead, only their annual energy consumption is known, which is used to scale standard load profiles (SLP). The scaled SLP values are then utilized by the SE as pseudo-measurements, and a constant power factor of 0.95 is assumed. In addition to the prosumer measurements and pseudo-measurements, a metering device is placed at the secondary side of the substation that measures the line-to-neutral voltage magnitude and the power flow on all four LV feeders. Further power flow measurements are taken at a remote cable distribution cabinet (cf. Fig. 3). Measurement noise is neglected, since its influence is presumably small compared to the large error introduced by pseudo-measurements.

We would like to point out here that the assumed SM measurement update rate of one second would not necessarily be supported by SMGWs available today. German legislation, for instance, only requires SMGWs to support measurement transmission for the purpose of grid state determination at least every minute [26]. Nonetheless, we deem that from the technical point of view, an update interval of one second is not an immoderate requirement.

### 3.3 Simulation timeframe, EV charging and priority setting

We choose one exemplary September day between 10 a.m. and 11 p.m. as the simulation timeframe. The maximum solar power time series data is derived from measurements of a PV plant in southern Germany that were taken within the research project *Verteilnetz 2020* [27]. With regards to EV charging, we assume that 28 of the 36 EVs arrive at their charging stations in the afternoon. The arrival times follow a standard distribution around 4:30 p.m. with 30 min. standard deviation. It should be noted that this level of concurrency is very high and reflects a worst-case scenario that is chosen to stress the operation management [28]. In addition, every 2nd of the arriving EVs only stays at the charger for a short time and leaves again around 7 p.m. for another ride. To account for the different charging durations, the priority factors of the EVs are gradually increased from 1 up to 6 at maximum when the next departure approaches and the SOC has not yet reached a target value of 80%.

## 4. Evaluation

To evaluate the operation management controller, its application to the use case described above is simulated in Matlab®/Simulink®. In doing so, the three-phase power flow equations are solved with a granularity of one second to obtain the true grid state, assuming rated voltage at the primary side of the substation transformer.

### 4.1 Simulation setup

In a first simulation, the proposed operation management controller computes DER active and reactive power set value updates each second. The step size parameters of the primal-dual algorithm (14a)–(14g) are set to  $\alpha = 100$ ,  $\alpha_v = 2.5$  and  $\alpha_i = 0.4$ . A communication network simulation handles the data exchange between DERs and the controller. It applies delays according to pre-computed probability distributions as described in Sect. 2.7. Furthermore, actual measurements are only available from prosumers containing DERs, and the power consumption of the remaining passive loads is estimated from SLPs as detailed in Sect. 3.2.

In a second simulation, the Matpower OPF function is employed each second to compute the updates of DER set values. In Matpower, cost functions can be assigned to DERs. For comparability, they are defined such that they match the utility functions (with opposite sign) described in Sect. 2.5. In contrast to the first simulation, exact values of all nodal powers are passed to the Matpower OPF without any delay, and DER power limits are assumed to be known. These prerequisites would not be fulfilled in a realistic setting – thus, the results from the Matpower OPF serve as benchmark values for our controller. On the basis of the simulation results, we aim to evaluate how close the proposed controller reaches the benchmark utility values, and how well the voltage and current constraints are met in spite of the imperfect measurements and the iterative nature of the online optimization. It should be noted here that instead of applying the voltage and current constraints to phase values as described in (1)–(2), only the positive sequence values are considered. The reason is that the Matpower OPF does not support unbalanced three-phase computations.

## 4.2 Simulation results

The results in terms of the actual DER power values as well as the positive sequence node voltages and the transformer current are shown in Fig. 4. The plots in the left column of Fig. 4 depict the results of the proposed operation management controller, which is referred to as *OnOpt-SE*. The corresponding benchmark results are shown in the right column (denoted by *MP*). We now utilize Fig. 4 to analyse the controller behaviour.

### 4.2.1 First period: PV injection

The DER actual active and reactive power values are plotted in Fig. 4(a)–(d) and comprise all PV plants and EV chargers, so they each contain 54 lines. Thus, they provide an overview rather than allowing for individual DER analysis. In (a)–(b), all power values greater than zero belong to PV plants, while negative values indicate EVs. It can be seen that the first half of the timeframe is dominated by PV power injection. It should be noted that visible fluctuations of the PV powers are due to varying solar irradiation rather than curtailment by the controller. Figure 4(c)–(d) show that both OnOpt-SE and MP employ PV reactive power consumption around 12:00, which is sufficient to keep the node voltages below the upper limit. This is depicted in Fig. 4(e)–(f), where the brightly shaded area indicates the range between node voltage minimum and maximum within the grid (highlighted by dark lines) and limits are marked by dotted lines. It is noticeable that the MP stops reactive power consumption around 14:00. The OnOpt-SE, on the contrary, reduces reactive power consumption rather slowly. This is due to the incremental gradient approach in combination with the very low cost assigned to reactive power, which results in very small gradient steps in (14e) once all voltage limit violations have been cleared.

### 4.2.2 Second period: EV charging

The second half of the timeframe is dominated by EV charging, which starts at 15:50 when the first EV arrives at its charging station. Figure 4(a)–(b) show that while the first EVs charge at nominal power of 11 or 22 kW, both OnOpt-SE and MP similarly curtail charging powers from app. 16:30 on to prevent the minimum node voltage from decreasing below the lower limit, as shown in (e)–(f). At the same time the transformer current, which is plotted in Fig. 4(g)–(h), reaches its limit (i.e. its rated value) of 360 A. From comparing left and right columns of Fig. 4(e)–(h), we conclude that the OnOpt-SE performs very well in keeping the voltage and current limits. In doing so, the active power curtailment is very similar to the benchmark values. On the contrary, quite a difference is noticeable in reactive power employment, which is depicted in Fig. 4(c)–(d). Both OnOpt-SE and MP utilize reactive power injection to support node voltages, but individual DER reactive power values highly differ in the MP results while reactive power is more evenly distributed among the DERs by the OnOpt-SE. The difference is likely to stem from the approximated voltage sensitivities to reactive power changes utilized in the OnOpt-SE, as described in Sect. 2.4. In view of the low reactive power cost, the effect on the overall utility is presumably low, which will be investigated in the following subsection. Again, once reactive power is not required any longer to keep voltages and currents within limits, which holds from approximately 20:00 on, the MP quickly reduces reactive power injection to zero. The OnOpt-SE reduces reactive power only slowly due to the small gradient steps associated with the low reactive power cost. Whereas this is not considered to be problematic, it could be counteracted by assigning higher costs to reactive power. On the other hand, too high costs for reactive power would provoke unintended active power curtailment.

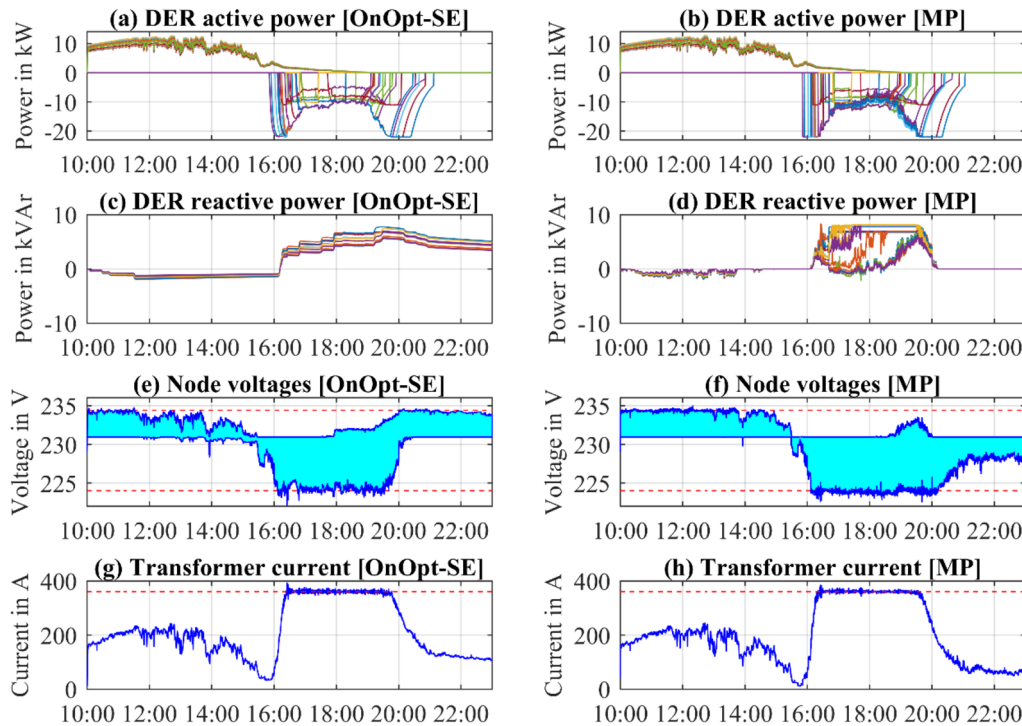


Fig. 4. Comparison of the proposed controller (OnOpt-SE, left column) and the Matpower OPF results (MP, right column). Voltages and currents refer to the positive sequence values

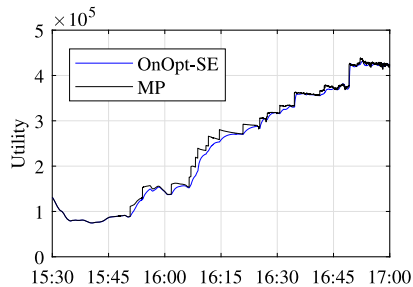


Fig. 5. Comparison of the overall DER utility reached by the OnOpt-SE in comparison to the Matpower benchmark (MP)

#### 4.2.3 Overall utility

In the above analysis, certain peculiarities of the OnOpt-SE have been identified, and we noticed that the performance of the operation management controller with regards to voltage and current limit adherence does not significantly differ from the benchmark algorithm in spite of the pseudo-measurement uncertainty and the iterative nature of the OnOpt-SE. Now, we intend to evaluate how close the OnOpt-SE gets to the MP result in terms of the overall utility, i.e. the target function value  $\Phi_{tot}$  according to (11). The MP value is considered as the “gold standard” that could theoretically be achieved.

To this end, Fig. 5 depicts the overall utility computed on the basis of the actual DER power values in each second between 15:30 and 17:00, which is a critical period as the EVs arrive at their charging stations and require a control action. The plots show that the utility obtained by the OnOpt-SE almost perfectly follows the benchmark results with only little delay, which results from the iterative procedure that prevents rapid changes of the power set values. Here, the

fast control cycle of only one second pays off: in spite of the small gradient steps taken in each timestep, it does not take long for the OnOpt-SE to arrive at the new equilibrium after the conditions have changed (e.g. an EV arrives and starts charging).

Therefore, we deem that the online optimization is indeed a favourable method in this application: with a simple control law, it quickly converges towards an optimal value similar to an omniscient offline optimization algorithm. Even if the latter was applicable (necessitating e.g. that DER power limitations were known), in a realistic setting it would reasonably be implemented with a larger control cycle in view of the optimization complexity. This would imply that it could not react to rapid changes of the boundary conditions, e.g. dropping PV power due to cloud cover, as fast as the online optimization. The benefits of the online optimization come at the cost of requiring a rapid communication of measurement and control values. In this regard, our results show that the LTE network modelled in Sect. 2.7 is capable of carrying the communication load. Neither packet delays nor packet losses significantly influenced the OnOpt-SE performance.

#### 5. Conclusion

In this article, we have proposed an operation management for unbalanced three-phase LV distribution grids with a high number of controllable DERs. Key characteristics of the proposed method are as follows:

- The *utility* of DER power injection and consumption is quantified, and its maximization is formulated as the optimization objective. This way, a fair allocation of limited grid capacity is strived for.
- The optimization problem is solved by an *online optimization* algorithm that requires a high update rate and thus a powerful communication network, but keeps the controller complexity low.



- A LV grid state estimation is included to account for different measurement values and to allow the control of grid state variables that are not directly measured.

The simulation results presented show that in the exemplary use case, the proposed operation management controller achieves similar results in terms of the overall utility and the constraint adherence like the benchmark OPF. By utilizing an LTE radio network, the required high update rate is supported. At the same time, the controller features lightweight algorithms that enable its implementation on low-cost hardware.

Thinking towards a real-world implementation from a technical point of view, most of today's LV grids are lacking important prerequisites to apply the proposed control. For example, the smart meter rollout in Germany is still in the initial phase; also, smart meters are not obliged to transmit measurements with an update rate shorter than 60 seconds [26]. Another challenge is that the grid topology and impedance data need to be at least approximately known to apply the SE, although the results in [8] indicate a certain robustness of the SE against model errors. In addition, at least a few measurement devices to complement the smart meters should be installed to accurately estimate the grid state. However, with increasing SM distribution and communication network establishment, we deem that some of these hurdles will be overcome in the next years.

Apart from the technical aspects, the utility formulation is also worth discussing. Within this article, we restricted the investigation to EVs and PV plants. In our future research, we intend to extend the controller applicability by including further types of DERs and also the power flow to or from the superordinate MV grid into the utility formulation. Furthermore, we plan to develop a distributed implementation of the utility-based operation management and investigate its performance under DER and communication network failures.

### Acknowledgement

This work has been funded by the Deutsche Forschungsgemeinschaft (DFG, German Research Foundation) under project number 426655646.

**Funding Note** Open Access funding enabled and organized by Projekt DEAL.

**Publisher's Note** Springer Nature remains neutral with regard to jurisdictional claims in published maps and institutional affiliations.

**Open Access** Dieser Artikel wird unter der Creative Commons Namensnennung 4.0 International Lizenz veröffentlicht, welche die Nutzung, Vervielfältigung, Bearbeitung, Verbreitung und Wiedergabe in jeglichem Medium und Format erlaubt, sofern Sie den/die ursprünglichen Autor(en) und die Quelle ordnungsgemäß nennen, einen Link zur Creative Commons Lizenz beifügen und angeben, ob Änderungen vorgenommen wurden. Die in diesem Artikel enthaltenen Bilder und sonstiges Drittmaterial unterliegen ebenfalls der genannten Creative Commons Lizenz, sofern sich aus der Abbildungslegende nichts anderes ergibt. Sofern das betreffende Material nicht unter der genannten Creative Commons Lizenz steht und die betreffende Handlung nicht nach gesetzlichen Vorschriften erlaubt ist, ist für die oben aufgeführten Weiterverwendungen des Materials die Einwilligung des jeweiligen Rechteinhabers einzuholen. Weitere Details zur Lizenz entnehmen Sie bitte der Lizenzinformation auf <http://creativecommons.org/licenses/by/4.0/deed.de>.

### References

- Richardson, P., Flynn, D., Keane, A. (2010): Impact assessment of varying penetrations of electric vehicles on low voltage distribution systems. In IEEE PES general meeting (pp. 1–6). New York: IEEE Press. <https://doi.org/10.1109/PES.2010.5589940>.
- Aziz, T., Ketjoy, N. (2017): PV penetration limits in low voltage networks and voltage variations. IEEE Access, 5, 16784–16792. <https://doi.org/10.1109/ACCESS.2017.2747086>.
- Bundesamt für Justiz (2016): Gesetz über die Elektrizitäts- und Gasversorgung (Energiewirtschaftsgesetz – EnWG), §14a Steuerbare Verbrauchseinrichtungen in Niederspannung; Verordnungsermächtigung. [https://www.gesetze-im-internet.de/enwg\\_2005/\\_14a.html](https://www.gesetze-im-internet.de/enwg_2005/_14a.html), gesehen am 08.07.2021.
- Bernstein, A., Dall'Anese, E. (2019): Real-time feedback-based optimization of distribution grids: a unified approach. IEEE Trans. Control Netw. Syst., 6, 1197–1209. <https://doi.org/10.1109/TCNS.2019.2929648>.
- Gan, L., Low, S. H. (2016): An online gradient algorithm for optimal power flow on radial networks. IEEE J. Sel. Areas Commun., 34, 625–638. <https://doi.org/10.1109/JSAC.2016.2525598>.
- Ortmann, L., Hauswirth, A., Caduff, I., et al. (2020): Experimental validation of feedback optimization in power distribution grids. Electr. Power Syst. Res., 189, 106782. <https://doi.org/10.1016/j.epsr.2020.106782>.
- Picallo, M., Bolognani, S., Dörfler, F. (2020): Closing the loop: dynamic state estimation and feedback optimization of power grids. In Power systems computation conference 2020, Porto, Portugal.
- Ipach, H., Stock, S., Becker, C. (2021): A modified branch-current based algorithm for fast low voltage distribution grid state estimation using smart meter data. In ETG congress 2021 (pp. 1–6).
- Heuck, K., Dettmann, K., Schulz, D. (2013): Elektrische Energieversorgung. 9. ed. Heidelberg: Springer. <https://doi.org/10.1007/978-3-8348-2174-4>.
- Dghim, H., El-Naggar, A., Erlich, I. (2018): Harmonic distortion in low voltage grid with grid-connected photovoltaic. In 2018 18th international conference on harmonics and quality of power (ICHQP) (pp. 1–6). New York: IEEE Press. <https://doi.org/10.1109/ICHQP.2018.8378851>.
- Helm, S., Hauer, I., Wolter, M., et al. (2020): Impact of unbalanced electric vehicle charging on low-voltage grids. In 2020 IEEE PES innovative smart grid technologies Europe (ISGT-Europe) (pp. 665–669). <https://doi.org/10.1109/ISGT-Europe47291.2020.9248754>.
- Abur, A., Expósito, A. G. (2004): Power system state estimation: theory and implementation. New York: Dekker. ISBN 0-8247-5570-7.
- Primadianto, A., Lu, C.-N. (2017): A review on distribution system state estimation. IEEE Trans. Power Syst., 32, 3875–3883. <https://doi.org/10.1109/TPWRS.2016.2632156>.
- Handschin, E. (1987): Elektrische Energiesysteme. 2. ed. Heidelberg: Hüthig. ISBN 3-7785-1401-6.
- Bolognani, S., Zampieri, S. (2016): On the existence and linear approximation of the power flow solution in power distribution networks. IEEE Trans. Power Syst., 31, 163–172. <https://doi.org/10.1109/TPWRS.2015.2395452>.
- Montoya, O. D., Gil-González, W. (2020): On the numerical analysis based on successive approximations for power flow problems in AC distribution systems. Electr. Power Syst. Res., 187, 106454. <https://doi.org/10.1016/j.epsr.2020.106454>.
- Ipach, H., Becker, C. (2020): Utility-optimizing real-time congestion management in low voltage distribution grids. In 2020 IEEE PES innovative smart grid technologies Europe (ISGT-Europe) (pp. 685–689). New York: IEEE Press. <https://doi.org/10.1109/ISGT-Europe47291.2020.9248878>.
- Zimmerman, R. D., Murillo-Sanchez, C. E., Thomas, R. J. (2011): MATPOWER: steady-state operations, planning, and analysis tools for power systems research and education. IEEE Trans. Power Syst., 26, 12–19. <https://doi.org/10.1109/TPWRS.2010.2051168>.
- Soerries, B., Lucidi, S., Nett, L., Wissner, M. (2019): Gutachten Digitalisierung der Energiewende – Tophema 3: TK-Netzinfrastruktur und TK-Regulierung.
- Seack, A., Kays, J., Rehtanz, C. (2014): Generating Low Voltage Grids on the Basis of Public Available Map Data. CIRED Workshop Rome, 11–12 June 2014.
- Fisser, L., Timm-Giel, A. (2021): Minimizing age of information for distributed control in smart grids. In 2021 IEEE international conference on communications, control, and computing technologies for smart grids. Accepted for publication.
- Pretico, G., Gangale, F., Mengolini, A., et al. (2016): Distribution system operators observatory: from European electricity distribution systems to reference network. EUR 27927 EN. <https://doi.org/10.2790/701791>.
- Meinecke, S., Sarajlić, D., Drauz, S. R., et al. (2020): SimBench—a benchmark dataset of electric power systems to compare innovative solutions based on power flow analysis. Energies, 13, 3290. <https://doi.org/10.3390/en13123290>.
- Tjaden, T., Bergner, J., Weniger, J., Quaschnig, V. Repräsentative elektrische Lastprofile für Einfamilienhäuser in Deutschland auf 1-sekündiger Datenbasis, Datensatz, Hochschule für Technik und Wirtschaft (HTW) Berlin, Lizenz: CC-BY-NC-4.0.
- Gesetz zur Digitalisierung der Energiewende (2016): Bundesgesetzblatt Jahrgang 2016 Teil I Nr. 43, ausgegeben zu Bonn am 1. September 2016: [https://www.bmwi.de/Redaktion/DE/Downloads/Gesetz/gesetz-zur-digitalisierung-der-energiawende.pdf?\\_\\_blob=publicationFile&v=4](https://www.bmwi.de/Redaktion/DE/Downloads/Gesetz/gesetz-zur-digitalisierung-der-energiawende.pdf?__blob=publicationFile&v=4), gesehen am 08.07.2021.
- Bundesamt für Sicherheit in der Informationstechnik (2019): Errata für die BSI TR-03109-1 V1.9.1 – TAF 9 und TAF 10. Version 1.0. <https://www.bsi.bund.de/>

[SharedDocs/Downloads/DE/BSI/Publikationen/TechnischeRichtlinien/TR03109/TR-03109-1\\_Errata-TAF9-TAF10.pdf](#). Accessed 11 August 2021.

27. Mauermann, H., Dietz, A., Maucher, B., Gamper, P., Witzmann, R., et al. (2019): Abschlussbericht zum Verbundvorhaben Verteilnetz 2020. <https://mediatum.ub.tum.de/doc/1524654/1524654.pdf>, gesehen am 08.07.2021.

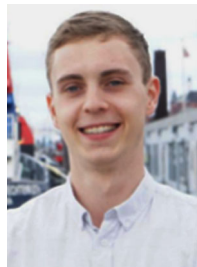
28. Verband der Bayerischen Energie- und Wasserwirtschaft e.V. – VBEW (ed.) (2019): VDE-Hinweis E-Mobilität: Netzanschluss und Netzverträglichkeit von Ladeeinrichtungen. Ausgabe 04.2019.

## Authors



### Hanko Ipach

is currently a research assistant at the Institute of Electrical Power and Energy Technology at Hamburg University of Technology, Germany, since 2017. He received his B.Sc. from the University of Hamburg in 2012 and his M.Sc. from the Technical University of Munich in 2014. Before joining the iiet, he worked as a project engineer at Wärtsilä SAM Electronics in Hamburg. His research interests include monitoring and optimization algorithms for power distribution grids.



### Leonard Fisser

received his Bachelor of Science in Electrical Engineering at the Hamburg University of Technology in 2017 through a dual study program. In 2019, he received his Master of Science in Electrical Engineering with distinction while specializing in telecommunications and communications engineering. He wrote his thesis on "Predictive Resource Allocation in Shared Spectrum Radio Systems" at the Institute of Communication Networks (ComNets). Since 2020 Leonard Fisser is a research assistant and PhD candidate at the ComNets Institute of Prof. Timm-Giel at the Hamburg University of Technology where he is focusing his research on Smart Grid Communication Systems.



### Christian Becker

is a full professor and head of the Institute of Electrical Power and Energy Technology at Hamburg University of Technology, Germany, since 2015. He received his Dipl.-Ing. degree in 1996 and his Dr.-Ing. degree in 2001 at TU Dortmund University. From 2002 to 2015 he worked in the R&D division of Airbus. His research activities and professional experiences are focused on power system stability and control engineering for terrestrial as well as on-board electrical power systems with dedicated focus on grid integration of power electronics equipment and FACTS.



### Andreas Timm-Giel

is heading the Institute of Communication Networks at TUHH as full professor since 2009. Previously, he was with MediaMobil GmbH and M2SAT Ltd. as Technical Project Leader and Manager Network Operations and with the Communication Networks group at the University of Bremen. In 2014, he was appointed Vice President of Research, TUHH. In 2021, he was appointed as TUHH President. His research interests include mobile and vehicular communications, sensor networks, IoT, network planning and the future internet.